Identification of a gain-of-function mutation in a Golgi P-type ATPase that enhances Mn^{2+} efflux and protects against toxicity

Somshuvra Mukhopadhyay and Adam D. Linstedt[1]

Department of Biological Sciences, Carnegie Mellon University, Pittsburgh, PA 15213

Edited by Jennifer Lippincott-Schwartz, National Institutes of Health, Bethesda, MD, and approved December 7, 2010 (received for review September 14, 2010)

P-type ATPases transport a wide array of ions, regulate diverse cellular processes, and are implicated in a number of human diseases. However, mechanisms that increase ion transport by these ubiquitous proteins are not known. SPCA1 is a P-type pump that transports Mn^{2+} from the cytosol into the Golgi. We developed an intra-Golgi Mn^{2+} sensor and used it to screen for mutations introduced in SPCA1, on the basis of its predicted structure, which could increase its Mn^{2+} pumping activity. Remarkably, a point mutation (Q747A) predicted to increase the size of its ion permeation cavity enhanced the sensor response and a compensatory mutation restoring the cavity to its original size abolished this effect. In vivo and in vitro Mn^{2+} transport assays confirmed the hyperactivity of SPCA1-Q747A. Furthermore, increasing Golgi Mn^{2+} transport by expression of SPCA1-Q747A increased cell viability upon Mn^{2+} exposure, supporting the therapeutic potential of increased Mn^{2+} uptake by the Golgi in the management of Mn^{2+}-induced neurotoxicity.

manganese | membrane trafficking | secretion | GPP130

P-type ATPases are ubiquitously expressed proteins that mediate transport of a wide array of cations and phospholipids and thereby regulate diverse cellular processes (1). The Na^+/K^+ ATPase generates membrane potential in neuronal cells, the sarco/endoplasmic reticulum Ca^{2+} ATPase (SERCA) regulates skeletal muscle contraction, the H^+/K^+ ATPase mediates gastric acidification, and lipid flippases transport phospholipids to the outer leaflet of the plasma membrane. P-type pumps share a high degree of sequence, structural and functional similarity, and their varied substrate specificities arise from minor changes in their ion-binding residues. During ion transport, autophosphorylation at an invariant aspartic acid residue in the cytoplasmic domain induces a characteristic conformation change from the E1 state, which has high affinity for the ion, to the E2 state, which has low affinity for the ion (1–4). Transport through these pumps is limited by the rate of this conformational change (2). Devising molecular techniques that can increase ion transport through P-type ATPases will significantly improve our understanding of cellular processes regulated by these pumps and may also contribute to new treatments of diseases related to these processes.

Secretory pathway Ca^{2+} ATPase1 (SPCA1) is a Golgi-localized P-type ATPase, which pumps Ca^{2+} from the cytosol into the Golgi and plays an important role in regulating Ca^{2+} homeostasis in mammalian cells (5). Haploinsufficiency of SPCA1 results in the development of Hailey-Hailey disease, a blistering dermatosis associated with increased cytosolic Ca^{2+} levels and impaired Ca^{2+} signaling in keratinocytes (5–7). Whereas much attention has been focused on its Ca^{2+} transport activity, SPCA1 can also transport Mn^{2+} into the Golgi with the same affinity as Ca^{2+} (4, 8). The Mn^{2+} transport activity of SPCA1 is particularly important because mechanisms regulating Mn^{2+} homeostasis in mammalian cells are unknown. Furthermore, whereas Mn^{2+} is an essential element required for the catalytic activity of a wide array of enzymes (5), at elevated levels, Mn^{2+} competes with magnesium-binding sites in proteins, enhances oxidative stress, compromises mitochondrial function, and eventually induces apoptosis (5, 9–11). The cytotoxic effects of Mn^{2+} result in the development of manganism, a Parkinson-like neurodegeneration syndrome, in adults and cognitive and behavioral defects in children (12–14). Thus, identifying mechanisms that reduce cytosolic Mn^{2+} levels during elevated exposure is of high clinical significance.

Blocking uptake of extracellular Mn^{2+} is unlikely to succeed in protecting against Mn^{2+} toxicity because, in mammalian cells, extracellular Mn^{2+} is transported into the cytosol by multiple ion pumps and channels that belong to different protein families and are not specific for Mn^{2+}. However, increasing $Mn2^{+}$ pumping into the Golgi could potentially reduce cytosolic Mn^{2+} levels and thereby protect against toxicity. Unfortunately, the role of the mammalian Golgi in Mn^{2+} detoxification has thus far not been tested for three principal reasons. First, compartment-specific subcellular Mn^{2+} sensors have not yet been identified, making it impossible to rapidly screen for conditions increasing Mn^{2+} transport into the Golgi. Second, the Golgi localization of SPCA1 is saturable and overexpression of the wild-type (WT) protein results in its accumulation in endosomes. Third, as there are no known mechanisms to increase the ion transport through P-type ATPases, it has not been possible to increase the Mn^{2+} transport activity of SPCA1.

In the current study we used the predicted structure of SPCA1 to generate mutations that could potentially increase its Mn^{2+} pumping activity. Using a unique in vivo Golgi-specific Mn^{2+} sensor to rapidly screen for conditions that increase Golgi Mn^{2+}, we identified Q747A as a point mutation that increased the Mn^{2+} transport activity of SPCA1. Analysis indicated that the structural basis for the enhanced activity of SPCA1-Q747A was increased size of its ion permeation cavity revealing, an unexpected contribution of ion permeation to the overall rate of transport through a P-type ATPase. Furthermore, expression of SPCA1-Q747A protected cells from the cytotoxic effects of Mn^{2+}, indicating that conditions increasing Mn^{2+} transport into the Golgi may be therapeutically useful in the management of manganism.

Results

Golgi Phosphoprotein of 130 kDa (GPP130) is an Intra-Golgi Mn^{2+} Sensor. To rapidly screen for conditions that increased Golgi Mn^{2+} uptake in vivo, we needed a sensor that specifically responded to increased Mn^{2+} within the Golgi lumen. Although compartment-specific Mn^{2+} sensors have not been described, we recently reported that exposure of cells to as low as 100 μM of Mn^{2+} induces the *cis*-Golgi glycoprotein, GPP130, to traffic from the Golgi to multivesicular bodies (MVBs) and then to lysosomes, where it is degraded (15). Fig. 1*A* shows the Mn^{2+}-induced redistribution and degradation response of GPP130 relative to

Author contributions: S.M. and A.D.L. designed research; S.M. performed research; S.M. analyzed data; and S.M. and A.D.L. wrote the paper.

The authors declare no conflict of interest.

This article is a PNAS Direct Submission.

[1]To whom correspondence should be addressed. E-mail: linstedt@cmu.edu.

This article contains supporting information online at www.pnas.org/lookup/suppl/doi:10.1073/pnas.1013642108/-/DCSupplemental.

the Golgi marker giantin. To test whether this response was triggered by an increase in Mn^{2+} in the Golgi lumen, we depleted SPCA1 to block transport of Mn^{2+} from the cytoplasm into the Golgi. Knockdown of SPCA1 abolished the Mn^{2+}-induced redistribution and degradation of GPP130 (Fig. 1 *B–D*). Gene replacement with full-length SPCA1 restored the Mn^{2+} response of GPP130, whereas replacement with a mutated version defective in autophosphorylation (D350A) and thus unable to transport either Mn^{2+} or Ca^{2+} (2, 16) did not (Fig. 1 *E* and *F*). Furthermore, replacement with SPCA1 containing a mutation (G309C) that blocks Mn^{2+} but not Ca^{2+} pumping activity (4) also failed to rescue the Mn^{2+} response of GPP130 (Fig. 1 *E* and *F*). Thus, the Mn^{2+}-induced degradation of GPP130 required a specific increase in intra-Golgi Mn^{2+} levels, indicating that GPP130 could be used to screen for conditions that increase Golgi Mn^{2+}.

Identification of SPCA1-Q747A as a Potential Hyperactive Mn^{2+} Transporter. We first tested whether overexpression of SPCA1-WT increased Golgi Mn^{2+} uptake. However, the Golgi localization of SPCA1 was saturable and the level of pump activity increased by WT overexpression did not detectably enhance GPP130 degradation when compared with untransfected cells (Fig. 2*A*). Another possibility was to increase the Mn^{2+} pumping activity of SPCA1. A mutation was created (Q747A) to reduce the side chain size of a residue predicted to line the Mn^{2+} permeation cavity (see below) as this might improve access of Mn^{2+} ions to the ion-binding site in SPCA1. Remarkably, expression of SPCA1-Q747A induced GPP130 degradation even in the absence of externally added Mn^{2+} (Fig. 2 *A* and *B*), suggesting a hyperactivated pump. Degradation of GPP130 was confirmed by immunoblot and the loss induced by SPCA1-Q747A corresponded to the transient transfection frequency (Fig. 2*C*). To test whether SPCA1 triggered the GPP130 response due to its Mn^{2+} pumping activity, we introduced into SPCA1-Q747A mutations that block pump activity (D350A) or block Mn^{2+} but not Ca^{2+} transport (G309C) and observed that these mutations blocked its ability to induce GPP130 degradation (Fig. 2 *A* and *B*). Although endogenous SPCA1 was present in these experiments, it was not required as loss of GPP130 induced by SPCA1-Q747A was also observed in cells lacking endogenous SPCA1 due to knockdown (Fig. S1).

SPCA1-Q747A expression did not affect Golgi morphology or alter the localization and level of other tested Golgi proteins (Fig. S2 *A–D*). We also confirmed that SPCA1-Q747A did not alter protein trafficking between the Golgi and the endocytic or secretory pathways. Treatment of cells with monensin to block endosome-to-Golgi protein trafficking causes rapid endosomal accumulation of Golgi protein of 73 kDa (GP73), which constitutively cycles between the Golgi and endosomes (17). The level of the monensin-induced endosomal accumulation of GP73 did not differ between cells that expressed SPCA1-Q747A and those that did not (Fig. S2 *E–G*). Additionally, expression of SPCA1-Q747A did not alter the distribution or localization of LAMP-2 (Fig. S2 *H–J*), a protein that traffics to lysosomes from the Golgi (18). Finally, we analyzed endoplasmic reticulum-to-surface trans-

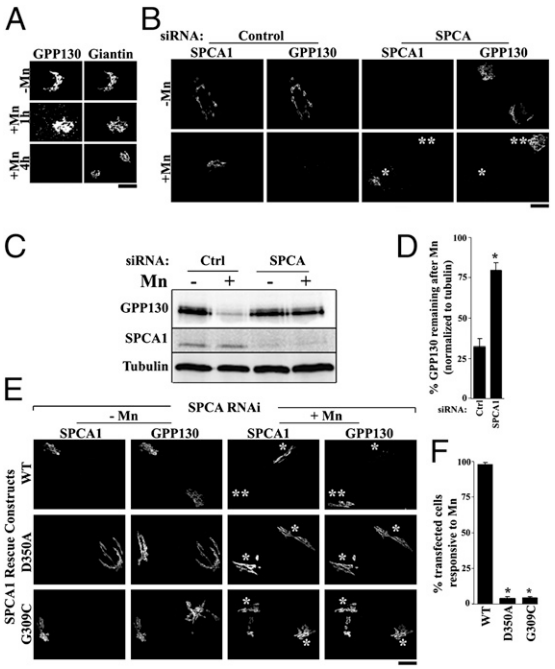

Fig. 1. Increased intra-Golgi Mn^{2+} induces degradation of GPP130. (*A*) HeLa cells were treated with 500 μM of Mn^{2+} for the indicated times and imaged to detect GPP130 and giantin. (Scale bar, 10 μm.) (*B*) Cells treated with control or anti-SPCA1 siRNAs for 48 h were transfected with HA-tagged SPCA1-WT and, after 24 h, were exposed to 500 μM of Mn^{2+} for 4 h and stained using anti-HA (to detect SPCA1) and anti-GPP130. After Mn^{2+}, GPP130 was degraded in cells transfected with the control siRNA as well as in cells in which SPCA1 was not depleted after knockdown (single asterisk). Cells with no detectable SPCA1 after knockdown did not exhibit Mn^{2+}-induced loss of GPP130 (double asterisk). (Scale bar, 10 μm.) (*C*) Levels of GPP130, myc-SPCA1-WT, and tubulin in cells treated exactly as described in *B* were determined by immunoblot. (*D*) Quantitation after immunoblotting to determine the levels of GPP130 remaining after Mn^{2+}, normalized to tubulin, in cells transfected with control or anti-SPCA1 siRNAs (mean ± SE; $n = 3$; $P < 0.05$). (*E*) Cells treated with anti-SPCA1 siRNA for 48 h were transfected with RNA-resistant HA-tagged SPCA1-WT or mutated constructs. After 24 h they were exposed to 500 μM of Mn^{2+} for 4 h and imaged to detect SPCA1 using an anti-HA antibody and GPP130. After Mn^{2+}, GPP130 was lost in cells expressing SPCA1-WT but not D350A or G309C (single asterisk). Knockdown cells not transfected with SPCA1-WT did not exhibit a GPP130 Mn^{2+} response (double asterisk). (Scale bar, 10 μm.) (*F*) Quantitation of percentage of transfected cells that did not have detectable GPP130 after Mn^{2+} from *E* (mean ± SE; $n = 100$ cells per experiment from three independent experiments; $P < 0.05$).

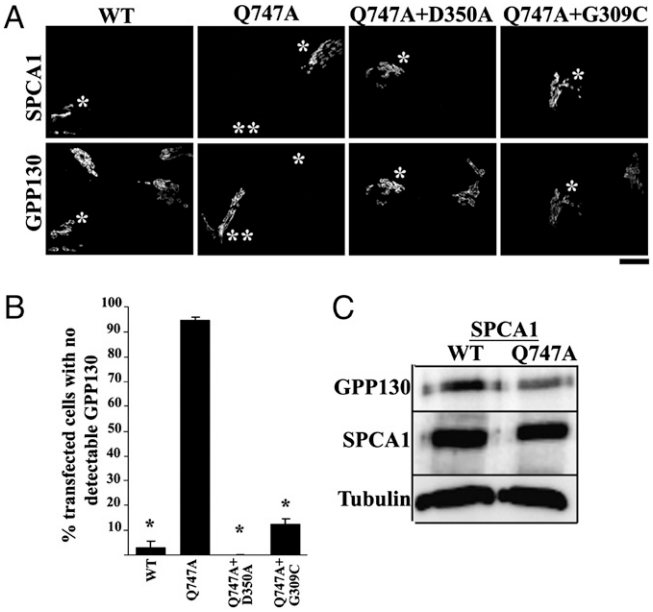

Fig. 2. SPCA1-Q747A enhances the GPP130 Mn^{2+} response. (*A*) HeLa cells were transfected with HA-tagged SPCA1-WT or mutated constructs and 24 h later imaged to detect HA and GPP130. GPP130 was degraded in cells transfected with SPCA1-Q747A but not WT or the double mutants (single asterisk). In the SPCA1-Q747A transfected culture, GPP130 was clearly detected in untransfected cells (double asterisk). (Scale bar, 10 μm.) (*B*) Quantitation of percentage of transfected cells without detectable GPP130 (mean ± SE; $n = 100$ cells per experiment from six independent experiments; $P < 0.05$). (*C*) HeLa cells were transfected with HA-tagged SPCA1-WT or Q747A and harvested 24 h posttransfection as described previously (15). Immunoblotting was performed to detect GPP130, HA, and tubulin.

port of the temperature-sensitive mutant of vesicular stomatitis virus G protein (VSVG) tagged with GFP (19, 20). VSVG-GFP trafficking in cells expressing SPCA1-Q747A was indistinguishable from controls, in each case reaching the Golgi in 20 min and the cell surface in 60 min (Fig. S3).

We also determined that SPCA1-Q747A induced GPP130 degradation by the pathway we previously described for Mn^{2+}-induced GPP130 degradation (15). Upon SPCA1-Q747A expression, GPP130 trafficked to peripheral punctae that overlapped with Rab7, a marker for MVBs, and LAMP-2 before degradation (Fig. S4 *A* and *B*). GPP130 was also detected within the lumen of giant MVBs induced by coexpression of Rab5-Q79L (Fig. S4*C*). Coexpression of dominant negative Rab7 (Rab7-T22D), which inhibits MVB-to-lysosome trafficking, blocked the GPP130 degradation, whereas dominant negative Rab5 (Rab5-S34N), which blocks early endosome-to-MVB trafficking, did not (Fig. S4 *D–F*). In cells coexpressing SPCA1-Q747A and Rab7-T22D, GPP130 accumulated in large peripheral punctae (Fig. S4 *D–F*), consistent with our previous description of the retention of GPP130 in an enlarged MVB compartment in Mn^{2+}-treated cells expressing Rab7-T22D (15). Thus, using GPP130 as an intra-Golgi $Mn2^{+}$ sensor, we identified SPCA1-Q747A as a potentially hyperactive $Mn2^{+}$ transporter.

Substitution of Q747 with Alanine Increases Activity of SPCA1 by Increasing the Size of the Ion Permeation Cavity. SPCA1 is >70% similar to SERCA in its transmembrane domains (21). Mutagenesis and computational modeling of SPCA1 on the basis of the known SERCA structure (22–25) indicate that SPCA1 has a single ion-binding site located between the fourth and sixth transmembrane domains (M4 and M6) and formed by E-308, N-738, and D-742 (2, 4, 26) (Fig. 3*A*). The most likely route for ions to reach this site is through the cavity between M4 and M6. Indeed, this route is taken by hydrated Ca^{2+} to reach a similarly positioned ion-binding site in SERCA (22) and mutations in residues of M4 and M6 block access of ions to the homologous ion-binding site in Pmr1p (21, 27, 28). Residue Q747 of SPCA1 is predicted to be at the cytoplasmic/membrane interface of M6 with an orientation that projects its side chain into the solvent accessible cavity between M4 and M6 (Fig. 3 *A–C*). On the basis of our modeling of SPCA1, the minimum distance or gap between M4 and M6 at this ion entrance point, occurring between V313 on M4 and Q747 on M6, was 3.89 Å (Fig. 3*D*). Analysis of a recomputed structure of SPCA1 containing the Q747A substitution confirmed that the side chain volume of residue 747 projecting into the cavity was reduced (Fig. 3*E*). As a consequence, the corresponding distance between M4 and M6 increased to 7.0 Å and the apparent minimum distance in the ion permeation cavity, which now occurred between V313 and G743, was 4.86 Å (Fig. 3*E*). The increase in gap between M4 and M6 induced by the Q747A substitution is significant in comparison to the ~1.6Å diameter of a hydrated Mn^{2+} ion (29) and could significantly increase the rate at which Mn^{2+} reaches the ion-binding site and thus enhance overall pumping activity of SPCA1. Indeed, rate increases are observed in potassium channels containing mutations that increase the size of their transport cavities (30, 31).

As a test of whether the increase in distance between M4 and M6 caused the gain-of-function observed in SPCA1-Q747A, we attempted to restore the WT distance in SPCA1-Q747A by substituting isoleucine for V314 on M4. According to our modeling of SPCA1, the V314I substitution rotated the side chain of V313 bringing it to within 3.6 Å of G743 on M6 and created a minimum gap similar to WT (Fig. 3*F*). In contrast to the strong response of GPP130 to SPCA1-Q747A, the construct containing the compensatory mutation, SPCA1-Q747A+V314I, failed to induce GPP130 degradation (Fig. 3 *G* and *H*). This could not be attributed to a loss of activity because SPCA1-Q747A+V314I rescued the Mn^{2+} response of GPP130 in cells lacking endogenous SPCA1 due to knockdown (Fig. S5 *A* and *B*). As the V314I substitution suppressed the Q747A phenotype without reintroducing a polar side chain, it suggests that it is increased gap

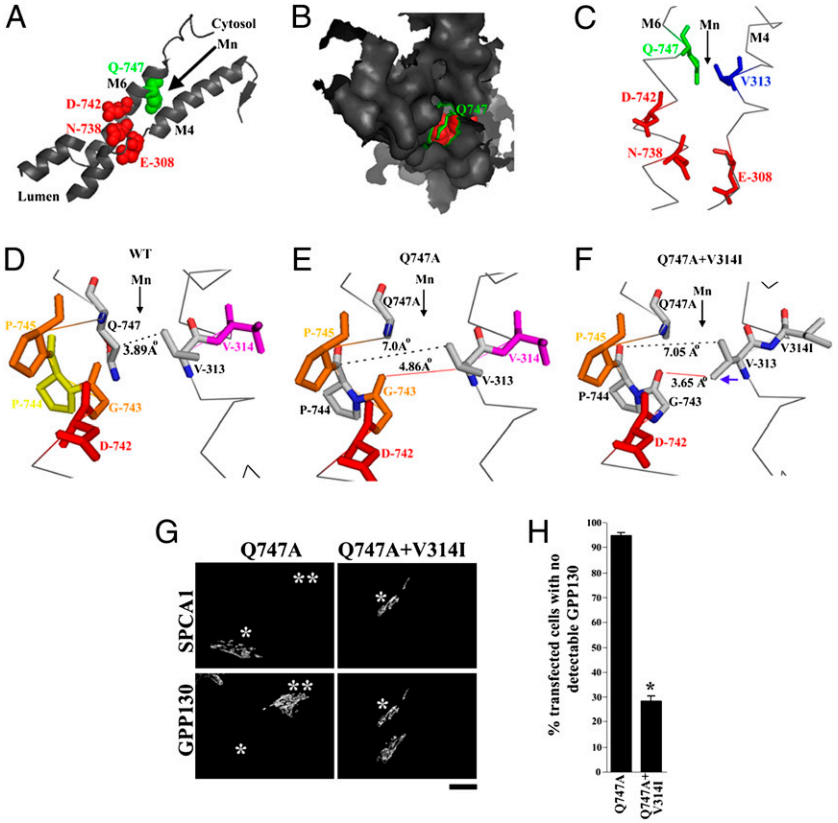

Fig. 3. The Q747A substitution increases the size of the SPCA1 ion permeation cavity. (*A–C*) SPCA1-WT was modeled using the MODBASE server as described in *Materials and Methods*. The M4 and M6 transmembrane domains are depicted in cartoon (*A*), surface (*B*), and ribbon (*C*) forms using the open source PyMol software. Ion-binding residues, E308, N738, and D742 are depicted in red; residue Q747 is in green; and V313 is in blue. Arrowheads indicate the path used by ions to reach the ion-binding site. (*D–F*). Distances across the ion permeation cavity are shown for the computed structures of SPCA1-WT, SPCA1-Q747A, and SPCA1-Q747A+V314I. Distances between M4 and M6 were measured using the "Measurement Wizard" in PyMol and the structures of the SPCA1 mutants were obtained using the "Mutagenesis Wizard" of PyMol. Blue arrowhead in *F* shows the rotation of the side chain of V313 after the V314I substitution. Black arrowheads indicate the likely path traversed by ions en route to the ion-binding site. (*G*) HeLa cells were transfected with HA-SPCA1-Q747A or HA-SPCA1-Q747A+V314I and imaged 24 h later to detect GPP130 and HA. GPP130 was degraded in cells transfected with SPCA1-Q747A but not in those expressing the V314I mutation (single asterisk). Untransfected cells in the SPCA1-Q747A transfected culture exhibited Golgi-localized GPP130 (double asterisk). (Scale bar, 10 μm.) (*H*) Quantitation of percentage of transfected cells lacking detectable GPP130 from *G* above (mean ± SE, $n = 50$ cells from four independent experiments, $P < 0.05$).

distance and not absence of partial charge that determines the ability of SPCA1-Q747A to increase Golgi Mn^{2+}.

Q747A Mutation Increases Mn^{2+} Pumping Activity of SPCA1. To directly test whether the Q747A mutation hyperactivated SPCA1, we performed an in vitro $^{54}Mn^{2+}$ uptake assay on Golgi membranes isolated from cells expressing SPCA1-WT and SPCA1-Q747A. Immunoblotting confirmed recovery of comparable levels of SPCA1-WT and SPCA1-Q747A in the respective pooled Golgi membranes (Fig. 4*A*) and uptake of $^{54}Mn^{2+}$ was specific as it was effectively competed by excess nonradioactive Mn^{2+} (Fig. 4*B*). Significantly, uptake of $^{54}Mn^{2+}$ was >80% higher in the Golgi vesicles containing SPCA1-Q747A (Fig. 4*B*), indicating increased pump activity. These assays lacked Ca^{2+}, thus increased Mn^{2+} transport was not due to blocked Ca^{2+} access to the ion-binding site. Indeed, uptake of $^{54}Mn^{2+}$ in SPCA1-Q747A containing Golgi vesicles was effectively competed by excess nonradioactive Ca^{2+} (Fig. S6*A*). Uptake was also carried out in permeabilized cells and again $^{54}Mn^{2+}$ uptake was specific (Fig. 4*C*) and the presence of SPCA-Q747A conferred a twofold increase (Fig. 4*D*). Finally, we used a pulse-chase assay to test whether SPCA1-Q747A increased Mn^{2+} transport into the Golgi in intact cells. Initial controls revealed that intracellular uptake of $^{54}Mn^{2+}$ progressively increased between 5 and 30 min and was effectively competed by addition of excess nonradioactive Mn^{2+} (Fig. 4*E*). During a subsequent 30-min chase incubation, intracellular $^{54}Mn^{2+}$ decreased by ~60% (Fig. 4*F*) as $^{54}Mn2^{+}$ was released into the medium (Fig. 4*G*). The release of $^{54}Mn^{2+}$ was blocked by pretreatment of the cells with brefeldin A, a fungal metabolite that blocks secretion (Fig. 4 *F* and *G*), indicating that the released $^{54}Mn^{2+}$ was secreted. The efflux of $^{54}Mn^{2+}$ was ~3%/min as ~30% of releasable $^{54}Mn^{2+}$ was secreted every 10 min (Fig. S6*B*), which is in accord with previous observations of rapid $^{54}Mn^{2+}$ efflux (32). Efflux of $^{54}Mn^{2+}$ was inhibited by blocking transport of Mn^{2+} into the Golgi via knockdown of SPCA1 (Fig. S6*C*) and by transferring cells to 20 °C (Fig. 4*H*), a temperature that blocks Golgi-to-plasma membrane trafficking (33). These observations indicate that efflux of intracellular Mn^{2+} was primarily mediated via its transport into the Golgi and secretion. In support of the Q747A mutation hyperactivating Mn^{2+} pumping into the Golgi thereby promoting its release by secretion, cells expressing SPCA1-Q747A retained 20% less $^{54}Mn^{2+}$ and secreted 20% more than WT (Fig. 4 *I* and *J*).

SPCA1-Q747A Increases Cell Viability During Mn^{2+} Toxicity. On the basis of the finding that SPCA1-Q747A sequestered and then secreted more Mn^{2+}, we tested whether expression of this construct protected cells exposed to toxic levels of Mn^{2+}. A dose–response was carried out on control cells, indicating that exposure to 1 mM of Mn^{2+} for 16 h reduced viability by ~70% (Fig. 5*A*). Using this condition, the viability of cells expressing SPCA1-WT or Q747A was compared with control transfected cells. Cells expressing SPCA1-Q747A exhibited a 70% greater survival rate than those expressing the WT protein (Fig. 5*B*). The magnitude of increased viability was comparable to that of increased Mn^{2+} transport by SPCA1-Q747A. Furthermore, SPCA1-WT, which failed to increase Mn^{2+} transport (Fig. 4), also did not increase viability (Fig. 5*B*). On the other hand, knockdown of SPCA1, which reduced Mn^{2+} efflux, reduced cell viability by ~70%, highlighting the crucial role of Golgi Mn^{2+} uptake in mediating Mn^{2+} detoxification (Fig. 5*C*). To confirm the protective effect of Q747A on a cell-by-cell basis, control and Mn^{2+}-treated cells were imaged to identify transfected cells and score their viability. Untreated cells expressing SPCA1-WT or Q747A, as indicated by a transfection marker, were healthy in appearance and negative for staining with propidium iodide, which is excluded by viable cells (Fig. 5*D*). In contrast, most Mn^{2+}-treated cells expressing SPCA1-WT exhibited perturbed morphologies and were inviable, on the basis of propidium iodide staining (Fig. 5 *D* and *E*). Significantly, a large protective effect was again evident for SPCA1-Q747A as ~60% of cells expressing this construct remained

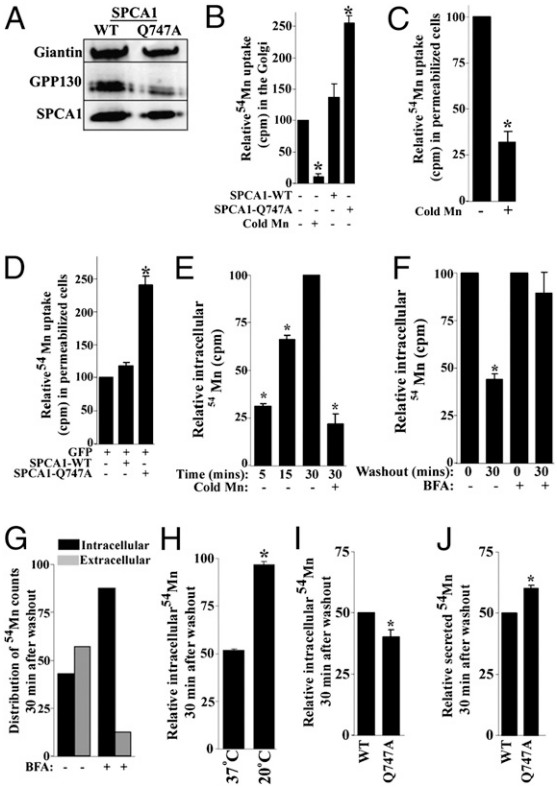

Fig. 4. SPCA1-Q747A is a hyperactive Mn^{2+} transporter. (*A*) Golgi membranes were isolated from cells transfected with HA-SPCA1-WT or Q747A as described in *Materials and Methods* and 2 μg of total protein was immunoblotted to detect giantin, GPP130, and HA. (*B*) Uptake of $^{54}Mn^{2+}$ by isolated Golgi vesicles was performed as described in *Materials and Methods*. Uptake was normalized to the uptake by untransfected cells (set to 100) and the experiment was replicated three times (mean ± SE; $P < 0.05$ for the difference in uptake in untransfected cells with and without excess cold Mn^{2+} and for the difference in uptake between SPCA1-WT and Q747A). (*C*) Uptake of $^{54}Mn^{2+}$ in permeabilized cells was done as described in *Materials and Methods*. Uptake in absence of cold Mn^{2+} was normalized to 100 for each experiment (mean ± SE, $n = 3$, $P < 0.05$). (*D*) Uptake of $^{54}Mn^{2+}$ on FACS sorted cells expressing either GFP alone or GFP and SPCA1-WT or GFP and Q747A was performed as in *C* above. Uptake in cells expressing GFP alone (set to 100) was used for normalization (mean ± SE, $n = 3$, $P < 0.05$ for the difference between SPCA1-WT and Q747A). (*E*) Cells were loaded with $^{54}Mn^{2+}$ and intracellular radioactivity was measured at various time points. Uptake at 30 min (set to 100) was used for normalization (mean ± SE, $n = 3$, $P < 0.05$). (*F*) Control or BFA-treated cells were loaded with $^{54}Mn^{2+}$ for 30 min, washed, and chased for 30 min. Intracellular radioactivity after a 30-min loading was normalized to 100 for control and BFA (mean ± SE, $n = 3$, $P <$ 0.05 for the difference in intracellular radioactivity retained after the chase in control cultures). (*G*) Distribution of intracellular and extracellular radioactivity after a 30-min chase in the presence or absence of BFA. (*H*) Cells were loaded with $^{54}Mn^{2+}$ for 30 min at 37 °C, washed, and chased for 30 min at 37 °C or 20 °C. Intracellular radioactivity after a 30-min loading was normalized to 100 (mean ± SE, $n = 3$, $P < 0.05$ for the difference in intracellular radioactivity retained between 37 °C and 20 °C groups). (*I* and *J*) FACS sorted cells expressing SPCA1-WT or Q747A were loaded with $^{54}Mn^{2+}$ for 30 min and subsequently chased for an additional 30 min. Intracellular radioactivity retained and secreted after the 30-min chase was normalized to 50 for WT-expressing cells (mean ± SE, $n = 3$, $P < 0.05$ for the difference in radioactivity retained and radioactivity secreted between WT and Q747A).

healthy looking and viable (Fig. 5 *D* and *E*). The protective effect of SPCA1-Q747A was also confirmed in the neuronal PC-12 cell line (Fig. S7). Finally, to determine whether, after uptake into the Golgi, secretion of Mn^{2+} was essential for detoxification, the toxicity assay was performed at 20 °C to block secretion and, as shown above, Mn^{2+} efflux. Cell viability was unaffected at 20 °C in

PHYSIOLOGY

the absence of Mn^{2+} but, after exposure to Mn^{2+}, the protective effect of SPCA1-Q747A was no longer evident (Fig. 5*F*). Thus, Mn^{2+} efflux via uptake by the Golgi and secretion is essential for Mn^{2+} detoxification and increasing Mn^{2+} transport into the Golgi protects against Mn^{2+}-induced cytotoxicity (Fig. 5*G*).

Discussion

Mutations inhibiting transport through P-type pumps are often described but gain-of-function mutations are not. After confirming that the previously described Mn^{2+}-induced trafficking and degradation of GPP130 (15) requires a specific increase in intra-Golgi Mn, we used GPP130 as a sensor of intra-Golgi Mn^{2+} and identified Q747A as a hyperactivating mutation of SPCA1. Structural modeling indicated that the Q747A substitution increased ion permeation to the binding site, which is significant because the rate of conformational change between the E1 and E2 states is considered rate limiting for P-type ATPases (2). It is unlikely that the Q747A substitution directly influenced the rate of this conformational change because Q747 does not appear to interact with neighboring residues in any of the SPCA1 conformations computationally determined on the basis of SERCA. A more likely possibility, based on the compensatory mutation, is that access to the ion-binding site is partially impeded by Q747 and reducing the size of Q747 allows quicker reloading of the pump when it reverts back to the E1 conformation.

There are a few known mutations of P-type ATPases that increase activity but these mutations relieve negative regulation to restore constitutive activity (34–36). The best-characterized example is for plasma membrane calcium ATPase (PMCA), which has an autoinhibitory domain that binds calmodulin (35, 36). Deletion of this domain increases Ca^{2+} transport to the level normally seen when calmodulin binds and counteracts the effect of the inhibitory domain (36).

Enlargement of the ion access cavity may be a generally applicable strategy to increase the intrinsic rates of P-type ATPases. Sequence alignments indicate that residues with bulky side chains are present at the entrance face of ion permeation cavities of other P-type pumps. Residues corresponding to Q747 of SPCA1 include T804 in SERCA and L888 in PMCA4. Conceivably, alanine substitution at these sites could hyperactivate the pumps. However, success in increasing pump activity would also depend on the nature of the other residues lining the cavity. For example, a mutation homologous to Q747A in the yeast homolog of SPCA1, Pmr1p (the mutation in Pmr1p is Q783A), blocks rather than increases Mn^{2+} transport (21, 27). This difference in activity likely occurs because, in contrast to the valine at 313 opposite Q747 in SPCA1, Pmr1p has an isoleucine in this position. The bulkier side chain of isoleucine may alter helix packing when present opposite the alanine residue in Pmr1p-Q783A and thereby occlude access of Mn^{2+} to the ion-binding site (21, 27). Thus, although using the SERCA structure to target the ion access gateway of other P-type ATPases is now an exciting possibility, careful attention will need to be paid to differences in neighboring residues.

Increased Mn^{2+} transport into the Golgi by SPCA1-Q747A protected cells against Mn^{2+}-induced cytotoxicity, whereas blocking Mn^{2+} transport into the Golgi or out of the Golgi to the cell surface had the opposite effect, showing the importance of the Golgi apparatus in Mn^{2+} homeostasis and detoxification in mammalian cells. Consistent with our results, HEK293 cells, which express low levels of endogenous SPCA1 (2), were recently shown to be sensitive to Mn^{2+} and protected from toxicity by SPCA1 expression (37). The identification of the Golgi as the major route of Mn^{2+} detoxification is significant, given that Mn^{2+} efflux via bile is the sole mechanism for Mn^{2+} excretion in humans, and patients with compromised liver function due to diseases like cirrhosis develop Mn-induced neurotoxicity without exposure to elevated Mn^{2+} (38). These results are also consistent with the Mn^{2+} hypersensitivity of Δ*PMR1* yeast strains (39) but, without a hyperactive Mn^{2+} pump, earlier investigations were unable to address whether increasing Mn^{2+} uptake into the Golgi offered any protective effect. Our findings reveal that increased Golgi Mn^{2+} uptake actually leads to less Mn^{2+} retention by cells due to secretion. Thus, increased pumping into the Golgi likely alters ion flux such that, at least within a particular concentration range of extracellular Mn^{2+}, efflux of Mn^{2+} becomes greater than influx.

Our results highlight the therapeutic potential of increasing cytosol-to-Golgi Mn^{2+} transport in the management of manganism, a disease that remains incurable. Clearly, gene therapy with SPCA1-Q747A is not easily feasible, but a promising avenue is a drug targeting the machinery responsible for SPCA1 locali-

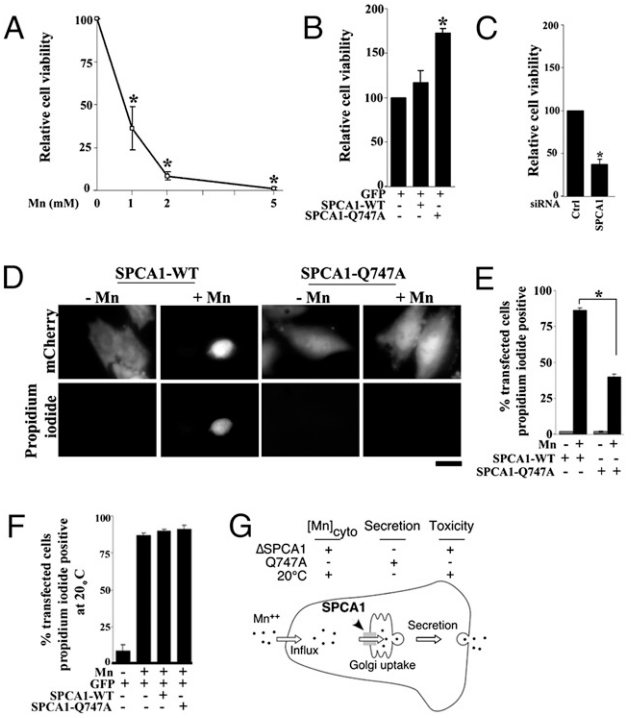

Fig. 5. Expression of SPCA1-Q747A protects cells from Mn^{2+} toxicity. (*A*) HeLa cells were exposed to 1, 2, and 5 mM of Mn^{2+} for 16 h and viability was determined using the MTT assay. Controls were untreated (0 mM of Mn^{2+}). Samples were normalized using absorption at 570 nm of the controls (set to 100) for each experiment (mean ± SE, $n = 3$, $P < 0.05$). (*B*) FACS sorted cells expressing GFP alone, GFP and SPCA1-WT, or GFP and SPCA1-Q747A were left untreated or exposed to 1 mM of Mn^{2+} for 16 h and viability was determined using the MTT assay. Viability in cells expressing GFP alone (set to 100) was used for normalization (mean ± SE, $n = 3$, $P < 0.05$ for the difference in viability between SPCA1-WT and Q747A). (*C*) Cells were treated with control or anti-SPCA1 siRNAs for 48 h and then exposed to 0 or 1 mM of Mn^{2+} for 16 h. Cell viability was assessed using the MTT assay and viability in cells treated with the control siRNA (set to 100) was used for normalization (mean ± SE, $n = 3$, $P < 0.05$ for the difference in viability between control and anti-SPCA1 siRNA treated groups). (*D*) Cells were transfected with SPCA1-WT or Q747A and mCherry for 24 h and then exposed to 1 mM of Mn^{2+} for 16 h. Propidium iodide staining was performed as described in *Materials and Methods*. (Scale bar, 10 μm.) (*E*) Quantitation of percentage of transfected cells positive for propidium iodide from *D* above (mean ± SE, $n = 25$ cells from three independent experiments per group, $P < 0.05$ for the difference between SPCA1-WT and Q747A after Mn^{2+}). (*F*) Cells were transfected with a GFP marker alone or cotransfected with GFP and SPCA1-WT or Q747A for 24 h and then exposed to 1 mM of Mn^{2+} for 16 h at 20 °C. Control cultures did not receive Mn^{2+}. Cell viability was then assayed using propidium iodide staining (mean ± SE, $n = 25$ cells from three independent experiments per group, $P > 0.05$ for the difference in cell viability between GFP, SPCA1-WT, and Q747A after Mn^{2+} and $P < 0.05$ for the difference in cell viability with and without Mn^{2+} in the GFP group). (*G*) Schematic showing that Mn^{2+} detoxification is mediated via transport into the Golgi in mammalian cells. Increasing Golgi Mn^{2+} uptake reduces cytosolic Mn^{2+} and protects against Mn^{2+} toxicity. Decreasing transport of Mn^{2+} into or out of the Golgi has the opposite effect.

zation in the Golgi. We observed that Golgi targeting of SPCA1 is readily saturated leading to endosome localization. Interestingly, a pool of endosomal SPCA1 has recently been detected in bile canalicular WIF-B cells (37), suggesting that SPCA1 in a physiologically relevant cell type may already be expressed in excess of that required for Golgi saturation. Thus, preventing SPCA1 exit from the Golgi in these cells should protect against Mn^{2+} toxicity.

In conclusion, we have elucidated an unexpected mode of hyperactivating the pumping activity of a P-type ATPase and demonstrated that increased Mn^{2+} pumping into the Golgi protects mammalian cells from the cytotoxic effects of Mn^{2+}.

Materials and Methods

Cell culture, transfections, immunofluorescence microscopy, image analysis, and immunoblot analyses were done as described by us previously (15, 19, 20, 40, 41). Tertiary structure of SPCA1 was derived using the algorithms of the MODBASE server (http://modbase.compbio.ucsf.edu/modbase-cgi/index.cgi; ref. 42). Purification of Golgi membranes on discontinuous sucrose gradients was done essentially as described (43, 44). The in vitro uptake of $^{54}Mn^{2+}$ in pooled Golgi membranes was done as described (16). To ensure 100% transfection frequency of SPCA1-WT or Q747A in a transient transfection system, cells were cotransfected with SPCA1-WT or Q747A and Rab5-GFP-WT and sorted using fluorescence-activated cell sorting (Vantage SF; Becton Dickinson) in the GFP channel. FACS sorted cells were used for uptake assays using permeabilized cells and for the viability assays using methylthiazolylphenyl-tetrazolium bromide (MTT). Uptake of $^{54}Mn^{2+}$ in permeabilized cells was done as described (4, 45). MTT assay was performed as described (15). Propidium iodide was from Sigma-Aldrich and was used as described by the manufacturer. See *SI Materials and Methods* for details.

ACKNOWLEDGMENTS. We thank Yehuda Creeger for help with the FACS assays; Claudia Almaguer for performing transfections in the PC-12 cells; Collin Bachert, Tina Lee, and Manojkumar Puthenveedu for critical reading of the manuscript; Donald R. Smith (University of California, Santa Cruz, CA) for advice; and Rajini Rao (The Johns Hopkins Medical School, Baltimore, MD) for sharing of unpublished data. This work was funded by National Institutes of Health Grant R01 GM-084111 (to A.L.).

1. Kühlbrandt W (2004) Biology, structure and mechanism of P-type ATPases. *Nat Rev Mol Cell Biol* 5:282–295.
2. Dode L, et al. (2005) Functional comparison between secretory pathway Ca2+/Mn2+-ATPase (SPCA) 1 and sarcoplasmic reticulum Ca2+-ATPase (SERCA) 1 isoforms by steady-state and transient kinetic analyses. *J Biol Chem* 280:39124–39134.
3. Dode L, et al. (2006) Dissection of the functional differences between human secretory pathway Ca2+/Mn2+-ATPase (SPCA) 1 and 2 isoenzymes by steady-state and transient kinetic analyses. *J Biol Chem* 281:3182–3189.
4. Fairclough RJ, et al. (2003) Effect of Hailey-Hailey disease mutations on the function of a new variant of human secretory pathway Ca2+/Mn2+-ATPase (hSPCA1). *J Biol Chem* 278:24721–24730.
5. Missiaen L, et al. (2004) SPCA1 pumps and Hailey-Hailey disease. *Biochem Biophys Res Commun* 322:1204–1213.
6. Sudbrak R, et al. (2000) Hailey-Hailey disease is caused by mutations in ATP2C1 encoding a novel Ca(2+) pump. *Hum Mol Genet* 9:1131–1140.
7. Missiaen L, Dode L, Vanoevelen J, Raeymaekers L, Wuytack F (2007) Calcium in the Golgi apparatus. *Cell Calcium* 41:405–416.
8. Ton VK, Mandal D, Vahadji C, Rao R (2002) Functional expression in yeast of the human secretory pathway Ca(2+), Mn(2+)-ATPase defective in Hailey-Hailey disease. *J Biol Chem* 277:6422–6427.
9. Milatovic D, Zaja-Milatovic S, Gupta RC, Yu Y, Aschner M (2009) Oxidative damage and neurodegeneration in manganese-induced neurotoxicity. *Toxicol Appl Pharmacol* 240:219–225.
10. Roth JA, Horbinski C, Higgins D, Lein P, Garrick MD (2002) Mechanisms of manganese-induced rat pheochromocytoma (PC12) cell death and cell differentiation. *Neurotoxicology* 23:147–157.
11. Zhao P, et al. (2008) Manganese chloride-induced G0/G1 and S phase arrest in A549 cells. *Toxicology* 250:39–46.
12. Olanow CW (2004) Manganese-induced parkinsonism and Parkinson's disease. *Ann N Y Acad Sci* 1012:209–223.
13. Wright RO, Amarasiriwardena C, Woolf AD, Jim R, Bellinger DC (2006) Neuropsychological correlates of hair arsenic, manganese, and cadmium levels in school-age children residing near a hazardous waste site. *Neurotoxicology* 27:210–216.
14. Bouchard M, Laforest F, Vandelac L, Bellinger D, Mergler D (2007) Hair manganese and hyperactive behaviors: Pilot study of school-age children exposed through tap water. *Environ Health Perspect* 115:122–127.
15. Mukhopadhyay S, Bachert C, Smith DR, Linstedt AD (2010) Manganese-induced trafficking and turnover of the cis-Golgi glycoprotein GPP130. *Mol Biol Cell* 21:1282–1292.
16. Sorin A, Rosas G, Rao R (1997) PMR1, a Ca2+-ATPase in yeast Golgi, has properties distinct from sarco/endoplasmic reticulum and plasma membrane calcium pumps. *J Biol Chem* 272:9895–9901.
17. Puri S, Bachert C, Fimmel CJ, Linstedt AD (2002) Cycling of early Golgi proteins via the cell surface and endosomes upon lumenal pH disruption. *Traffic* 3:641–653.
18. Shestakova A, Zolov S, Lupashin V (2006) COG complex-mediated recycling of Golgi glycosyltransferases is essential for normal protein glycosylation. *Traffic* 7:191–204.
19. Puthenveedu MA, Linstedt AD (2004) Gene replacement reveals that p115/SNARE interactions are essential for Golgi biogenesis. *Proc Natl Acad Sci USA* 101:1253–1256.
20. Yadav S, Puri S, Linstedt AD (2009) A primary role for Golgi positioning in directed secretion, cell polarity, and wound healing. *Mol Biol Cell* 20:1728–1736.
21. Mandal D, Rulli SJ, Rao R (2003) Packing interactions between transmembrane helices alter ion selectivity of the yeast Golgi Ca2+/Mn2+-ATPase PMR1. *J Biol Chem* 278:35292–35298.
22. Toyoshima C, Nakasako M, Nomura H, Ogawa H (2000) Crystal structure of the calcium pump of sarcoplasmic reticulum at 2.6 A resolution. *Nature* 405:647–655.
23. Toyoshima C, Nomura H (2002) Structural changes in the calcium pump accompanying the dissociation of calcium. *Nature* 418:605–611.
24. Toyoshima C, Nomura H, Tsuda T (2004) Lumenal gating mechanism revealed in calcium pump crystal structures with phosphate analogues. *Nature* 432:361–368.
25. Toyoshima C, Mizutani T (2004) Crystal structure of the calcium pump with a bound ATP analogue. *Nature* 430:529–535.
26. Ton VK, Rao R (2004) Functional expression of heterologous proteins in yeast: Insights into Ca2+ signaling and Ca2+-transporting ATPases. *Am J Physiol Cell Physiol* 287:C580–C589.
27. Mandal D, Woolf TB, Rao R (2000) Manganese selectivity of pmr1, the yeast secretory pathway ion pump, is defined by residue gln783 in transmembrane segment 6. Residue Asp778 is essential for cation transport. *J Biol Chem* 275:23933–23938.
28. Wei Y, et al. (2000) Phenotypic screening of mutations in Pmr1, the yeast secretory pathway Ca2+/Mn2+-ATPase, reveals residues critical for ion selectivity and transport. *J Biol Chem* 275:23927–23932.
29. Marcus Y (1983) Ionic-radii in aqueous-solutions. *J Solution Chem* 12:271–275.
30. Hänelt I, et al. (2010) Gain of function mutations in membrane region M2C2 of KtrB open a gate controlling K+ transport by the KtrAB system from Vibrio alginolyticus. *J Biol Chem* 285:10318–10327.
31. Xia M, et al. (2005) A Kir2.1 gain-of-function mutation underlies familial atrial fibrillation. *Biochem Biophys Res Commun* 332:1012–1019.
32. Aschner M, Gannon M, Kimelberg HK (1992) Manganese uptake and efflux in cultured rat astrocytes. *J Neurochem* 58:730–735.
33. Ladinsky MS, Wu CC, McIntosh S, McIntosh JR, Howell KE (2002) Structure of the Golgi and distribution of reporter molecules at 20 degrees C reveals the complexity of the exit compartments. *Mol Biol Cell* 13:2810–2825.
34. Curran AC, et al. (2000) Autoinhibition of a calmodulin-dependent calcium pump involves a structure in the stalk that connects the transmembrane domain to the ATPase catalytic domain. *J Biol Chem* 275:30301–30308.
35. Enyedi A, et al. (1989) The calmodulin binding domain of the plasma membrane Ca2+ pump interacts both with calmodulin and with another part of the pump. *J Biol Chem* 264:12313–12321.
36. Enyedi A, Verma AK, Filoteo AG, Penniston JT (1993) A highly active 120-kDa truncated mutant of the plasma membrane Ca2+ pump. *J Biol Chem* 268:10621–10626.
37. Leitch S, et al. (2010) Vesicular distribution of secretory pathway Ca(2+)-ATPase isoform 1 and a role in manganese detoxification in liver-derived polarized cells. *Biometals*, in press.
38. Aschner M, Erikson KM, Herrero Hernández E, Hernández EH, Tjalkens R (2009) Manganese and its role in Parkinson's disease: From transport to neuropathology. *Neuromolecular Med* 11:252–266.
39. Culotta VC, Yang M, Hall MD (2005) Manganese transport and trafficking: Lessons learned from Saccharomyces cerevisiae. *Eukaryot Cell* 4:1159–1165.
40. Sengupta D, Truschel S, Bachert C, Linstedt AD (2009) Organelle tethering by a homotypic PDZ interaction underlies formation of the Golgi membrane network. *J Cell Biol* 186:41–55.
41. Linstedt AD, Mehta A, Suhan J, Reggio H, Hauri HP (1997) Sequence and overexpression of GPP130/GIMPc: Evidence for saturable pH-sensitive targeting of a type II early Golgi membrane protein. *Mol Biol Cell* 8:1073–1087.
42. Pieper U, et al. (2006) MODBASE: A database of annotated comparative protein structure models and associated resources. *Nucleic Acids Res* 34(Database issue):D291–D295.
43. Xu H, Shields D (1993) Prohormone processing in the trans-Golgi network: Endoproteolytic cleavage of prosomatostatin and formation of nascent secretory vesicles in permeabilized cells. *J Cell Biol* 122:1169–1184.
44. Jesch SA, Linstedt AD (1998) The Golgi and endoplasmic reticulum remain independent during mitosis in HeLa cells. *Mol Biol Cell* 9:623–635.
45. Van Baelen K, Vanoevelen J, Missiaen L, Raeymaekers L, Wuytack F (2001) The Golgi PMR1 P-type ATPase of Caenorhabditis elegans. Identification of the gene and demonstration of calcium and manganese transport. *J Biol Chem* 276:10683–10691.